Bioelectric Characterization of Senescing Human Keratinocytes

Authors: Hamid Sediqi[1], Michael Levin[2,*]

Affiliations:

[1] Allen Discovery Center at Tufts University, Medford, MA 02155, USA.

*Corresponding author: michael.levin@tufts.edu

Running title: Bioelectrics of aging

Keywords: aging, resting potential, bioelectric pattern, in vitro, cell culture

Abstract

Aging, a ubiquitous process that affects almost all multicellular organisms, is accompanied by the accumulation of senescent cells, leading to a decline of morphology and function. The 'loss of morphostatic information' theory posits that aging occurs due to gradual breakdown of order initially established during embryo development. Spatial differences in cellular resting potential have many roles in organizing cell activity into complex anatomical structures during embryogenesis and regeneration. Thus, while bioelectric patterns are a good candidate for the information that degrades during aging, long-term changes in bioelectrical state in adult cells are not well-understood. Here, we sought to characterize the temporal and spatial bioelectric dynamics of human epidermal keratinocytes undergoing replicative senescence. We stained keratinocytes of varying ages using voltage sensitive dyes – BeRST, VoltageFluor 2.0 & 2.1 – and characterized p16 expression levels, senescence associated β-galactosidase activity, and chromatin condensation levels. Our results revealed senescence-associated membrane depolarization – consistent change of bioelectrical potential over the lifespan of cells. Moreover, we found increased heterogeneity of V_{mem} between cultures, reduced intra-culture variability, diminished cellular responsiveness to hyperpolarizing treatments, reduced resilience (ability to quickly and effectively achieve equilibrium post-perturbation), and degradation of multi-cellular patterns of bioelectric spatial organization. Modulation of resting membrane potential towards hyperpolarization abated, while depolarization exacerbated, senescence-associated phenotypes, demonstrating the instructive role of bioelectricity in replicative aging. These results reveal a breakdown of bioelectric patterning and regulation with senescence, consistent with the loss of morphostatic information theory of aging.

Introduction

Aging, the progressive decline of form and function, affects almost all multicellular organisms and [1, 2]. Many theories have been proposed to explain the cause of aging, and generally fall into two broad categories: damaged-based and programmatic-based. Damaged-based theories argue that aging occurs due to the accumulation of damage caused by oxidative stress, DNA damage, and the progressive malfunction of cellular repair mechanisms [3, 4]. Conversely, programmatic-based theories posit that aging is hardwired into the genome to give an evolutionary benefit at the cost of a limited lifespan [5, 6]. Despite much effort consistent with these hypotheses, there is a notable lack of definitive anti-aging treatments [7]. This led to the emergence of the Information-loss theory of aging which posits that aging is caused due to the progressive loss of biological information required to maintain homeostasis [8]. This loss of information is said to occur at the level of the epigenome – changes in the methylation profiles lead to epigenetic drift, reducing the fidelity of information driving cellular processes, and causing loss of cell identity [8].

Theories of aging focused on loss of information at the genetic (telomere) or epigenetic levels can explain changes in cellular properties. However, resistance to aging is a whole-body phenomenon that is likely connected to the overall processes of embryogenesis and regeneration. Resistance to aging is not something that is only needed later in life – it is likely part of the general machinery needed for a body to maintain order against the daily replacement of cells and the molecular noise that constantly threaten to disrupt tissue- and organ-level structures [9, 10]. Aging can be seen as the eventual failure of fundamental, ubiquitous mechanisms that organize cellular and molecular events toward the maintenance and repair of the target morphology and away from degeneration and cancer [11-13].

One possible cause of aging is progressive loss of Morphostatic Information [2]. During development, cellular collectives traverse the anatomical morphospace (the latent space of potential geometric configurations), to reach their target morphology - a region within that space that corresponds to the correct anatomy of a given species [14, 15]. Importantly, even after development into an adult, maintaining the final adult morphology is a highly active state that must counteract environmental stress and noise. It is likely that the key to longevity is understanding the computational processes enabling cellular collectives to establish and maintain order at various scales. What maintains the information needed for continuous upkeep of structure, within a specific region of morphospace over decades? A number of mechanisms have been implicated in on-going morphostasis, including dynamic biochemical and biomechanical gradients. Here we focus on endogenous bioelectricity: an important modality that has been implicated in large-scale morphogenetic control in embryogenesis, regeneration, and cancer suppression [16-18].

Endogenous bioelectrical signaling is driven by ion channels and pumps, present in all cells – not only neurons. The resting potential of cells regulates proliferation, migration, differentiation, and gene expression [19-28]. However, as in the brain, bioelectric signaling is not just a factor determining single cell behavior: due to electrical synapses known as gap junctions [29] and large-scale trans-epithelial electric fields [30, 31], tissue-level bioelectric states propagate and integrate across considerable distances in vivo. Spatial patterns of resting membrane potential have been shown to regulate the morphogenesis of the wing, eye, heart, limb, and brain in a range of model species and human patients (reviewed in [16-18, 32, 33]), and it is becoming clear that bioelectric regionalization provides an important underlying scaffold for defining tissue boundaries and organ-level structure [34]. Recent work has especially shown that a number of birth defects, induced both chemically and genetically, exert their teratogenic influence by blurring the endogenous bioelectric prepatterns that set the size and shape of the brain; moreover, the sharpness of these patterns are an attractive target for therapeutics because reinforcing the crisp boundaries between different bioelectric regions results in repair of severe defects of brain, gut, and heart [35-38]. Interestingly, cancer -

another loss of tissue-level order, which a human intact body must battle for decades [9, 39] – can likewise be induced by disruptions of endogenous bioelectric states and normalized by therapeutic restoration of V_{mem} and gap junctional connectivity [40-45].

While much work on V_{mem} patterns has occurred in various model systems [46, 47], less is known about human cells – a prerequisite for developing therapeutics. More generally, while resting potential of human cells, such as mesenchymal stem cells in culture [48-54], has been studied, it is not known what kind of multicellular patterns would exist in vitro – a scenario different from the cells' usual evolutionarily-established organ context, in which embryonic organizer processes are not available to regionalize V_{mem} patterns. Finally, the changes in bioelectric pattern over long timescales, beyond embryogenesis, are not well-characterized. Thus, here we sought to address these knowledge gaps by studying bioelectric states in human cells in vitro, during their natural process of senescence, using a state-of-the-art voltage dye visualization method that goes beyond first-generation bioelectric profiling methods [55, 56].

While there is a paucity of research into the role of bioelectricity in aging, some researchers have investigated ion channels and membrane potential changes in senescing cells. Plasma membrane depolarization has been suggested to be an important trigger for the induction of senescence [57-59], via depolarization as a result of increased expression of voltage-gated sodium channels [58, 59]. Knocking down these channels prevented the expression of p53 and the downregulation of mitotic genes [59]. Experiments exposing cells to depolarizing treatments were shown to exacerbate replicative aging and induce senescence [58, 59]. Together with the functional evidence for a role of bioelectric patterns in regenerative, embryonic, and neoplastic contexts [60, 61], these data suggest the importance of bioelectricity not only as a biomarker of aging, but also reveal it to have a functional role in cellular senescence.

Thus, we proposed a model in which loss of morphostatic information is specifically due to spatial bioelectric patterns' degrading with age, becoming blurred and thus making it more difficult for individual cells, even when replaced with new progeny, to take on appropriate system-level roles within the anatomical structure [1]. This model makes a number of non-mutually exclusive predictions, which we tested here: (a) is there an absolute shift in mean V_{mem} during senescence? (2) is there a reduction of precision (increase in variance) among cells as they age? (3) is there spatial order (separated domains of resting potential) which becomes less distinct over time? And (4) does cells' ability to respond to bioelectric signals [62], or resilience (time to return to equilibrium after perturbation) decline in senescence?

To explore these ideas, we used human keratinocytes isolated from the neonatal epidermis. Progenitor keratinocytes residing in the basal layer of the epidermis initially undergo proliferation, then differentiate while migrating towards the surface of the skin [63]. However, with increasing age, progenitor keratinocytes in the basal and spinous layer increasingly become senescent, reducing the skin's regenerative potential, thinning the epidermis, and impairing homeostasis [64]. As keratinocytes are the dominant cell type in skin, in vitro cultures provide researchers with a highly relevant model for studying skin aging processes such as senescence.

The present study aimed to determine the presence of age-dependent changes in the spatial patterning, responsiveness, and resilience of aging human epidermal keratinocytes' bioelectric states. We found that senescent-associated membrane depolarization is accompanied by increased bioelectric inter-culture and reduced intra-culture heterogeneity with respect to resting potential, diminished cellular responsiveness and resilience, as well as degradation of bioelectric spatial organization. Moreover, we report that modulation of resting membrane potential towards hyperpolarization abated senescence associated phenotypes, while depolarization exacerbated these phenotypes.

Methods

Cell Culture

To grow cells of varying ages, isolated Human Epidermal Keratinocytes-neonatal (HEK-n) (Science Cell Cat: 2100) were cultured in a T75 flask precoated with poly-L-lysine (Science Cell CAT: 0403) for 24-hours at 37ºC. Hek-n cells were kept in a humidified incubator at 37ºC and 5% CO_2 for 12 hours before being given fresh keratinocyte media (Science Cell CAT:2101). The cell culture media was replaced every two days until reaching 80% confluency, after which they were split into T75 flasks and grown until the desired age was reached, after which they were cryopreserved in keratinocyte media containing 10% DMSO.

Bioelectric Imaging of Resting Voltage Potential

A week prior to imaging, HEK-n cells were thawed from cryopreservation and cultured onto 10-cm^2 culture dishes containing 20-ml of keratinocyte media, and kept in a humidified incubator at 37ºC, and 5% CO_2 for 6-hours. The media was then replaced with fresh keratinocyte media to remove any traces of DMSO. Cells were cultured in a 96-well precoated with Poly-L Lysine at least 48-hours prior to V_{mem} characterization. Prior to timeseries imaging, cells were incubated with 600 nM of BeRST for 30 minutes, washed twice with PBS, and imaged with the Leica SP8 Confocal microscope for Fluorescence Lifetime characterization. FLIM images were acquired by exciting the BeRST dye at 658-nm and collecting the emission in the range of 681-nm – 800 nm. FLIM images were fitted with a biexponential decay curve, exported as '.Tif' files, then loaded into ImageJ for cell segmentation by 'Ostu' thresholding. Then the mean Lifetime was calculated for each cell. These data were then transferred to Prism GraphPad for graphing or R-studio for statistical testing.

Global and Local Moran's I – Calculation of Spatial Autocorrelation

To acquire FLIM images for spatial analysis, we used the V_{mem} sensitive Vf2.1 and the V_{mem} insensitive Vf2.0 dyes. The difference between these two fluorophores is that Vf2.0 lacks the aniline donor group which is crucial for voltage sensitivity. Consequently, this dye can be used to determine the contribution of any non-V_{mem} artifacts. For example, we found that using higher concentrations of VF2.0 led to quenching, consequently creating what appeared to be 'depolarized' regions in the culture. Reducing the concentration down to 50 nM of Vf2.0 gave rise to images that appeared to have a more random distribution of Lifetime values (Supplementary Figure 1). This concentration was then used to acquire large image cells with the voltage sensitive VF2.1 dye for spatial analysis.

To perform Moran's I computation, HEK-n cells of different ages were cultured in a flat bottom 96-well plate 24-hr prior to imaging. Cells were stained with 50 nM VF2.1 (ex: 488-nm, em: 500 – 700 nm) and with 1 µM of Hoechst (Ex: 405-nm, Em: 420 – 480 nm) for 30 minutes at 37ºC and 5% CO_2. Keratinocyte imaged with the Leica SP8 Confocal microscope paired with a 25x air Objective (refer to metadata of Leicha Image File for image settings/parameters). To generate centroid X, Centroid Y, and intensity values for each cell, background pixels were zeroed by creating masks via Otsu thresholding of intensity images, then applying the mask to the FLIM images. A python script was written to use a 15 x 15 pixel ROI to scan the image and only save X, Y, and Lifetime values of regions in the image that had no background pixels (i.e. pixel values >0). These data were then saved as a csv file. Prior to Moran's computation, an elbow test was performed to determine the appropriate k value which was revealed to be k=3. For this computation we subsampled our data using 1000 cells at a time and took the average over 10 iterations to account for differences in cell number.

Senescence Associated β-galactosidase characterization

Keratinocytes of varying ages were cultured onto a 96-well plate at least 48-hours prior to βGal characterization. Detection of SA-β-Gal was performed according to the manufacturer's specification (Cell Signaling Technologies, Cat: 9860). Briefly, cells were washed with PBS, fixed with the fixative solution, rinsed and then stained with the staining solution. Then the 96-well plate was sealed with parafilm to prevent evaporation prior to incubation for 24 hours in a dry incubator (no CO_2). The cells were then stained with Hoechst 3342 and imaged using EVOS M7000. Images of SA-β-Gal-stained cells were analyzed in ImageJ using the protocol developed by Krzystynial *et al* [65]. Their analysis involves color thresholding images to mask positively stained cells, then measuring the integrated density of the inversed image. This value is then divided by the number of nuclei to generate the 'integrated density of β Gal signal per cell'.

RT-qPCR

Total RNA was isolated using the Qaigen 'RNeasy Mini Kit' (Cat: 74104) according to manufacturer's instructions. To synthesize cDNA using 200 ng of isolated RNA, the Biorad Iscript cDNA synthesis (Cat: 1725035) kit was used. The expression level of $p16^{INK4A}$ mRNA was determined using PowerUp SYBR Green Master Mix (Fisher Scientific, Cat: A25777) using the following primers: FWD 'CTCGTGCTGATGCTACTGAGGA' and RVS GGTCGGCGCAGTTGGGCTCC'. The following PCR parameters were used: Activation: 50 °C for 2 min; Stage 2: pre-soak:95 °C for 10 min; Stage 3: Denaturation: 95 °C for 15 sec, Annealing: 60°C for 1 min; Stage 4: Melting curve: 95°C for 15 sec, 60°C for 15 sec, 95°C for 15 sec.

Absolute quantification of mRNA transcripts was performed using the Linear Regression of Efficiency method [66]. This approach works because during PCR the amplification efficiency progressively decreases as the amplicon concentration increases, and therefore, this reduction is linearly coupled to the amplicon DNA mass. For all RT-qPCR quantification, 100 femtograms of lambda DNA was used to as a standard to quantify p16INK4A mRNA.

Results

Senescent Keratinocytes Exhibit Depolarization, and Reduced Intra-culture, but Increased Inter-culture, V_{mem} Heterogeneity

To characterize the baseline bioelectrics of aging human epidermal keratinocytes, we imaged cells of different ages stained with 600 nM BeRST – a V_{mem} sensitive fluorophore [67-71]. BeRST is comprised of a silicon rhodamine fluorophore attached to a phenylvenevinylene molecular wire that is sensitive to changes in the electric field [55, 70]. The mechanism underpinning the voltage sensing involves photoinduced electron transfer (PeT). Staining cells with BeRST results in the molecular wire embedding into the plasma membrane, while the silicon rhodamine head resides on the surface. If the membrane potential is hyperpolarized the electron-rich molecular wire quenches the head, causing a reduction in fluorescence and Lifetime. Upon membrane depolarization, the PeT mechanism is disrupted, leading to an increase in fluorescence and Lifetime from the silicon rhodamine head [67, 68, 70, 71]. This dye provides important advantages over other voltage dyes currently being used. Firstly, it has a near-far red excitation, reducing photo-toxicity and enabling long-term live imaging. Secondly, since PeT underpins the voltage sensing mechanism of this dye – unlike other dyes that use the movement of a charged fluorophore in/out of the cell – the fluorescence intensity and Lifetime is not altered by changes in membrane permeability. This reduces artifacts introduced by differential dye uptake by cells.

Our results revealed significant depolarization of Keratinocytes upon reaching 40- ($p<0.05$, n=4 biological replicates) and 50-days ($p<0.05$, biological replicate n=13 biological replicates) in culture (Figure 1A) relative to 10-day old cells (n=9 biological replicates). This coincided with increased levels of three aging biomarkers: $p16^{INK4A}$ [72] expression, SA-β-galactosidase [73] activity, and chromatin condensation levels [74] ($p<0.05$, n=4 biological replicate; $p<0.0001$, n=6 biological replicate; $p<0.0001$, n=6 biological replicates). Moreover, the degree of V_{mem} heterogeneity between biological replicate cultures in a given age group, as measured by the size of standard deviation, became greater than 22-fold at day 40 and 15-fold at 50 days relative to 10-day old cells. In contrast, within each biological replicate, i.e. within a single culture, levels of heterogeneity were 38% lower in 50-day old (n=16 biological replicates) compared to 10-day ($p<0.0001$, n=9 biological replicates) old keratinocytes. Taken together, these data show that during senescence, keratinocytes undergo a change in the bioelectric state from polarization to depolarization which is accompanied by increased inter-culture V_{mem} heterogeneity and reduced intra-culture heterogeneity. These results show these bioelectric patterns as biomarkers of replicative senescence.

Senescent Keratinocytes are Less Responsive and Less Resilient to Induced Changes of V_{mem}

We next investigated age-dependent changes in responsiveness of keratinocytes to bioelectric signals, which is of relevance to both – design of external interventions via electroceutical drugs [46, 75-77] and the understanding of responsiveness of cells to endogenous bioelectric signals in vivo [34]. To trigger a V_{mem} change, we used the hyperpolarizing drug Pinacidil – a KATP channel activator [78]. We acquired images of keratinocytes stained with BeRST pre- and post-treatment to calculate the percentage change in Fluorescence Lifetime (Figure 3A). Keratinocytes progressively exhibited greater absolute percentage change in Lifetime, peaking on day 30 ($p<0.0001$, n=3 biological replicates). However, by day 40 keratinocytes appear to have the most diminished response level, albeit statistically not significantly different than day 10. In 50-day old senescent cultures, keratinocytes responded by depolarizing (Figure 3A) when exposed to pinacidil. These data show that keratinocytes become increasingly more responsive to Pinacidil treatment up to day 30; however, once they approach and achieve senescence (Figure 3A),

they become not only less responsive but also depolarize when given a hyperpolarizing stimulus.

To determine the presence of age-dependent changes in keratinocyte's resilience to V_{mem} perturbations, we calculated the level of time series' variance post treatment with Pinacidil. In system Dynamics, Resilience is the ability of a complex system to adapt to a new equilibrium post perturbation [1]. A system that is resilient will quickly and effectively adjust to a new setpoint, exhibiting little variance [1]; conversely, a frail system will struggle with adjusting to a new setpoint, exhibiting greater variance in their response. The Variance of each age group was calculated by using the standard deviation of each timeseries. This analysis revealed 50-day old cells with the highest level of variance compared to younger cells exposed to Pinacidil ($p<0.05$ day 10-day n=3 biological replicates, vs 50-day n=8 biological replicates). Furthermore, old senescent cultures immediately depolarized when given pinacidil followed by hyperpolarization, then a gradual progression towards depolarization. These data reveal that senescent cells have the lowest degree of V_{mem} resilience, and they fail to achieve a steady hyperpolarized state despite an initial attempt.

Senescent Keratinocytes Lose Ability to Form Distinct Bioelectric Domains

We next sought to determine whether cells in culture exhibit large-scale spatial regionalization with respect to V_{mem} (as observed in bioelectric patterns in vivo [61, 79, 80]) and whether this changes with age. To this end, we used the voltage insensitive 'VoltageFluor 2.0' and voltage sensitive 'VoltageFluor 2.1' which are analogs of BeRST. These fluorophores have a Sulfofluorescein rather than a rhodamine fluorophore so they are excitable with 488-nm light. The Vf2.0 dye lacks the aniline donor group which results in no PeT mechanism and is therefore not voltage sensitive. Using VF2.0 revealed concentration dependent quenching that gave rise to what appeared to be distinct voltage domains (Supplementary Figure 1). However, upon reducing the concentration down to 50 nM, the VF2.0 images appeared to have a more random distribution of Lifetime values (Supplementary Figure 1). This concentration was used to stain keratinocytes with VF2.1 for spatial autocorrelation characterization.

Surprisingly, we found that even *in vitro* - in the absence of exogeneous morphogenetic cues – the cells self-organized into domains (Figure 4). This was particularly apparent in 10-day old keratinocytes evident by the relatively high positive Global Moran's I of 0.5 (Figure 4A). This metric measures the degree of spatial autocorrelation – Moran's I value close to +1 indicates a strong positive spatial correlation, values close to zero indicate random spatial patterning, while negative values imply dissimilar values are adjacent [81]. Furthermore, to investigate whether aging affects Keratinocyte's bioelectric spatial organization, we computed Moran's Global and Local I for each age. This metric allowed us to quantify the spatial "sharpness" of bioelectric patterns – the crispness with which adjacent regions-maintained differences in V_{mem}. Compared to 10-day old cultures (n=10 biological replicates), a significant reduction in Moran's I from to 0.5 down to 0.13 in 40-day ($p<0.0001$, n=7 biological replicates) and 0.26 in 50-day old cells ($p<0.0001$, n=10 biological replicates) was observed. A reduction in linear regression was also observed when plotting the Lifetime values against spatially lagged Lifetime (Figure 5B-i) – the distribution of points became progressively more random with increasing age (Figure 5B-i). Moreover, computing and mapping Local Moran's I revealed a reduction in the size and distribution of distinct clusters with increasing age (Figure 5B-ii). Taken together these data show a loss of bioelectric spatial organization and reduced spatial heterogeneity (loss of ability to maintain coherent, distinct voltage regions) with increasing age.

Bioelectric Modulation of Keratinocytes Alters Senescence-Associated Phenotypes

To ascertain whether bioelectricity is a simple read-out of senescence rather than a highly relevant lever that can control cellular aging, we modulated keratinocyte resting membrane potential and characterized its impact on senescence biomarkers. To this end, we grew 30-day old cells an additional 6-days in either control media, media containing 10 μM Pinacidil or elevated potassium ion levels (+25 mM potassium gluconate). After 6 days, keratinocytes were cultured in fresh control media for 2 additional days until imaging. Figure 5A reveals a significantly higher number of cell nuclei in pinacidil treated ($p<0.0001$, n=18 biological replicates) and lower numbers in potassium gluconate treated cell cultures ($p<0.05$, n=24 biological replicates) relative to control cells (n=17 biological replicates). βGal staining revealed depolarizing treatment with potassium gluconate (n=6 biological replicates) increased levels of staining compared to control group ($p<0.001$, n=12 biological replicates). It was also apparent that despite the decrease in βGal staining levels of pinacidil treated cells, this difference was not statistically significant, likely due to the large standard deviation in the control group (Figure 5B). Notably, potassium gluconate treated cells appeared more solitary than control or pinacidil treated cells. This was especially apparent by cells heavily stained for βGal activity. This data suggests that senescent keratinocytes may have altered gap junctions which diminish their ability to bioelectrically communicate with each other. Analysis of chromatin condensation levels revealed significant decrease in pinacidil treated cells ($p<0.05$, control n=18 biological replicates, pinacidil n=16 biological replicates). Potassium gluconate treated cells appeared to have significantly higher levels of chromatin condensation ($p<0.0001$, n=2 biological replicate 3). Taken together, these data show hyperpolarization abates, while depolarization exacerbates, senescence markers.

To determine if hyperpolarization of keratinocytes also helped abate diminished cellular responsiveness associated with cellular senescence, we acquired timeseries images of keratinocytes pre- and post-treatment with Pinacidil. Our results revealed that keratinocytes pre-treated with pinacidil for 6 days exhibited the greatest degree of responsiveness ($p<0.01$, control n=4 biological replicates, Pinacidil n=3 biological replicates) when exposed to fresh media containing 10 uM of pinacidil (Figure 6A). Conversely, cells pre-treated with elevated potassium levels (+25 mM potassium gluconate) exhibited the lowest levels of responsiveness (n=3 biological replicates), albeit this diminished responsiveness was not statistically significant relative to the control group; however, it is suggestive. Notably, Figure 6B reveals that although pre-treated pinacidil cultures had the highest levels of responsiveness, they in fact progressively depolarized with time (Figure 6B). In contrast, pre-treated potassium cells appeared to initially depolarize but then progressively hyperpolarized when exposed to pinacidil. Control cells exhibited an initial recovery from depolarization, followed by oscillation near +10%. Taken together, these data reveal that while hyperpolarization abates diminished cellular responsiveness associated with senescence, the cellular response is altered so that cells depolarize when given hyperpolarizing stimulus.

We next investigate the impact of V_{mem} modulation on bioelectric spatial clustering and organization. Figure 7A reveals no significant difference between control cells and cells pre-treated with Pinacidil for 6 days. However, it appears that pre-treatment with elevated potassium ions significantly reduced Moran's I from 0.64 down to 0.26 ($p<0.01$, control n=4 biological replicates, potassium gluconate n=4 biological replicates). This is also evident in the Lifetime vs spatial lag Lifetime scatter plots which show that pre-treated potassium keratinocytes with a reduced R^2 value of 0.31 vs 0.67 in the control group, and by the more random distribution of points (Figure 7b-i). Performing local Moran analysis also revealed that the size and distribution of distinct clusters was significantly reduced (Figure 7b-ii). These data demonstrate that hyperpolarization via Pinacidil, did not significantly improve V_{mem} clustering, while depolarization significantly diminished keratinocytes' ability to self-organize in distinct V_{mem} domains.

Discussion

Here, we characterized bioelectric patterns associated with keratinocyte senescence. We determined the relative V_{mem} of keratinocyte stained with the voltage responsive dye – BeRST, while also quantifying aging biomarkers $p16^{INK4A}$ expression levels [72], senescence associated β-galactosidase activity [73], and senescence associated chromatin condensation. Our results revealed that keratinocytes significantly depolarize after 50 days in culture (Figure 1). This timepoint coincides with a significant increase in $p16^{INK4A}$ expression, β-galactosidase activity, and chromatin condensation levels (Figure 2). These data reveal depolarization as a biomarker of keratinocyte replicative senescence and is in agreement with previous research showing significant membrane depolarization as a crucial step for the induction of senescence [58, 59, 82].

We also found that the inter-culture heterogeneity of cells' V_{mem} values were significantly greater in 40 and 50-day old senescent keratinocyte cultures (Figure 1C). Paradoxically, we observed a significant reduction in intra-culture V_{mem} heterogeneity at 50 days relative to earlier timepoints. This suggests that biological replicates of older senescing cells will vary because some replicates would have already achieved senescence while others are still pre-senescent. However, possibly due to the loss of proliferative or differentiating cells, individual older senescing keratinocyte cultures exhibit more homogenous V_{mem} distributions within a given culture. While it is known that senescent cultures exhibit increased levels of cell-to-cell variability with respect to many aging biomarkers [83], the current study reports that old senescing keratinocytes exhibit reduced V_{mem} heterogeneity within the same culture and increased levels between replicate cultures.

Homeostatic processes, such as the ones that enable cells to cooperate towards reaching and maintaining a specific large-scale target morphology, can fail in one of several ways. For example, they can lose setpoint information, and/or, they can become unable to implement the error minimization steps even if the setpoint information is available to them. Thus, over time, one way in which the on-going maintenance of the body can be disrupted is through progressive degradation of bioelectrically-encoded information. Our data on V_{mem} changes during senescence is consistent with this. Another possible failure point of the morphological homeostasis cycle in vivo could be diminished responsiveness of individual cells to signals that drive collective behavior [2]. It is known that with increasing age cells have a reduced response to growth factors [84], hormones [85], immune signals [86], and even nutrients e.g. aged muscle cells show reduced sensitivity to amino acids such as leucine [87]. Here we investigated whether the ability to implement instructive bioelectrical signals likewise reduces over time, by determining cell's responsiveness to a V_{mem}-altering drug. We characterized, at different ages, the V_{mem} of cells pre- and post-treatment with Pinacidil – KATP agonist [78] (Figure 3). Results show that keratinocytes become increasingly more responsive to hyperpolarization until day 30; however, upon approaching and achieving senescing on 40 - 50 days of culture, a significant reduction in responsiveness is observed (Figure 3). In fact, it appears that 50-day old senescent cultures undergo depolarization rather than hyperpolarization when exposed to pinacidil. Immediately after exposure to pinacidil, 50-day old senescent cultures became depolarized and then they ostensibly attempt a correction with hyperpolarization; however, they seem unable to maintain a hyperpolarized state. This data suggests that even if senescing cells produce and receive the signals needed to maintain tissue-level bioelectrical order, they may be incapable of responding appropriately. If this phenomenon holds *in vivo*, then it would mean that senescent cells contribute to disrupting tissue homeostasis not only by their diminished responsivity to bioelectric/morphogenetic cues, but by executing the wrong response. The accumulation of these senescent cells in tissue would increasingly lead to aprogressive loss of morphostatic information stored in bioelectric gradients. These data also reveal that bioelectric interventions aiming to prevent senescence should target keratinocytes when they are most

responsive to hyperpolarization (30-days of culture) rather than attempting to rescue unresponsive senescent cells.

The resilience of a system is measured by how quickly and effectively it can converge or diverge from its equilibrium after perturbation [1]. Stochastic resilience theory incorporates the randomness of biological systems and therefore investigates the distribution of the system around equilibrium [1]. Here, we sought to investigate how the resilience of keratinocyte bioelectrics changes with age. One resilience metric is the variance of a timeseries after perturbation – greater variance indicates lower resilience [1]. To this end, we performed a time series acquisition pre- and post-treatment with Pinacidil. Our results revealed that 50-day old senescing cells exhibit the greatest degree of variance in V_{mem} (Figure 3B & C). These data reveal that senescent cells have significantly reduced resilience preventing them from quickly and effectively reaching a new homeostatic setpoint. The presence of such frail cells would expectedly introduce noise to the system, diminishing the ability to collectively coordinate their V_{mem}, and possibly reducing its ability to navigate through morphospace, because bioelectric patterns and their integration with downstream transcriptional and other mechanisms require significant temporal coordination to maintain longevity and optimal function.

The presence of frail senescent cells in culture or in tissue may consequently result in the degradation of instructive spatial bioelectric patterns. To investigate whether there were age-dependent differences in the spatial organization of bioelectric patterns, we computed Moran's Global and Local I, as well as linear regression analysis of Lifetime vs spatial-lag Lifetime for each age group. Moran's I, which ranges from -1 to +1, is a measure of spatial autocorrelation and consequently the degree of spatial clustering and organization present [81, 88]. A high Moran's I indicates strong spatial clustering of similar V_{mem} values; values closer to zero indicates randomness, and values close to negative one indicates negative clustering i.e. cells with dissimilar V_{mem} values neighbor each other. Computing Moran's I for keratinocytes of different ages revealed an age-dependent decrease in Moran's I, reaching the lowest degree in 40- and 50-day cultures. Plotting the Lifetime values of cells against the spatial lag-Lifetime values, which reveals whether there is strong linear regression, showed higher levels of linear regression in younger cells, and a progressive reduction with age, reaching the lowest at 40- and 50-days cultures. Moreover, computation and mapping of Local Moran's I showed a reduction in the size and distribution of distinct V_{mem} clusters with increasing age. Taken together, these data show that the bioelectric spatial organization of 2D culture of Keratinocytes significantly diminishes with age, providing further evidence for the morphostatic information loss theory of aging, in which the sharp differences between regions of different V_{mem} is blurred (as occurs during a number of birth defects [36-38, 89]). Notably, the reduction in Moran's I is consistent with the reduction in intra-culture variability – reduced variability (Figure 1C) would result in more homogenous and less distinct cell subpopulations. One notable feature of these data is that bioelectric regionalization exists at all, in vitro. While domains of different V_{mem}, demarcating developmental compartments, are well-known in the context of complex morphogenesis in vivo [61, 79, 90-95], it is surprising to find them in the absence of organizing centers. While the origin and significance of in vitro bioelectric patterns are as yet unknown, it is likely that they indicate the innate tendency of patterns to emerge via symmetry-breaking and self-organization in the excitable media of bioelectrically active and sensitive cells [96-100].

To determine whether bioelectricity plays an instructive role rather than just another biomarker of cellular senescence, we modulated the resting membrane potential of keratinocytes and characterized the impact on aging phenotypes. To this end, 30-day old keratinocytes were culture in either control media, hyperpolarizing media containing pinacidil or depolarizing media containing elevated levels of potassium ions (Figure 5). We found that hyperpolarizing keratinocytes for 6-days significantly increased

proliferation, and reduced chromatin condensation levels. Though it was not statistically significant due to the large standard deviation of control cells, pinacidil treated cells did appear to have almost a 50% drop in βGal staining levels. Depolarizing keratinocytes for 6-days resulted in decreased cell number, increased βGal activity and chromatin condensation levels. Taken together, these data demonstrate that hyperpolarization abates while depolarization exacerbates senescent associated phenotypes. These data are consistent with previous research showing hyperpolarization delaying the onset of aging biomarkers, while depolarization increased the expression of aging biomarker levels[58, 59].

We also observed that in the K^+Glu-treated cultures, keratinocytes appeared more disconnected from each other, particularly cells that exhibited higher βGal signal. Within K^+Glu cultures, cells that did not show high βGal staining appeared to still have connections and cluster together. This is reminiscent of cancer cells which become bioelectrically isolated from their neighbors and unresponsive to high order morphogenic cues [101]. Moreover, cancer cells are also significantly more depolarized compared to their wild-type counterparts [102, 103]. At first, it may seem paradoxical that depolarization in cancer cells leads to increased levels of proliferation [101], whereas depolarization in the context of senescence leads to growth arrest. However, it is possible that there is a different V_{mem} window required for senescence, and if cancer cells are pushed towards senescent V_{mem} values, they may undergo growth arrest. Indeed, research by Mathews *et al.* [101], show that chemical cocktail combinations (e.g. Temozolomide+NS1643, or Pantoprazole+Retigabine) which further depolarized U87 human glioblastoma cells also induced cellular senescence and growth arrest.

We next characterized pre-treated keratinocytes' responsiveness to ascertain whether modulation of the resting membrane potential also helped abate diminished cellular responsiveness associated with senescence (Figure 6A). Our results revealed that pre-treatment with hyperpolarization resulted in keratinocytes with the highest level of responsivity (Figure 6A). However, these cells underwent depolarization rather than hyperpolarization when given fresh pinacidil. This could be due to compensatory mechanisms activated during the chronic exposure to pinacidil over the 6-days. These data imply that future bioelectric modulations should possibly employ multiple hyperpolarizing drugs with different mechanisms of action to overcome the compensatory mechanisms of cells. Pre-treatment with depolarization resulted in the lowest responsivity; however, this was not statistically significant. Taking together, these data demonstrate that bioelectric interventions can abate senescent associated diminished responsivity.

We then characterized the spatial organization of cells pre-treated with depolarization or hyperpolarization (Figure 7). We expected that depolarization would lead to a reduction, while hyperpolarization to an increase in spatial V_{mem} clustering and organization. Our results show that compared to control cells, depolarization treatment did lead to significant reduction in spatial organization and clustering. However, Pinacidil treatment did not increase spatial autocorrelation but instead led to a non-statistically significant reduction. These data reveal that depolarization diminishes cells' ability to collectively organize and cluster in distinct V_{mem} domains, revealing a possible role of gap-junction disruption during senescence. Indeed, gap-junction (cx43) mRNA and protein levels are reportedly downregulated in aged Human umbilical vein endothelial cells[104] . Our data also reveals that treatment with pinacidil did not enhance spatial autocorrelation as expected. This may be due to the fact that pinacidil prevented the onset of senescence on an individual cell level but did not work to drive collective cell behavior.

Conclusion

The present study describes the bioelectrics of senescing keratinocytes, both in terms of the V_{mem} patterns they generate and in turn their ability to respond to bioelectric signals. We observed changes in both of these dimensions of anatomical homeostasis, consistent with the bioelectric emphasis of the 'Loss of Morphostatic Information' theory of aging [105]. Future work will explore bioelectric patterns, and the mechanisms that interpret changes therein, as potential targets for longevity therapeutics.

Acknowledgements:

We thank Evan W. Miller for his invaluable assistance with voltage imaging dyes, Patrick McMillian for his feedback on earlier drafts of this work, and Julia Poirier for assistance with the manuscript. M.L. gratefully acknowledges funding via sponsored research agreement with Astonishing Labs inc.

References

1. Cohen, A.A., et al., *A complex systems approach to aging biology.* Nature Aging, 2022. **2**(7): p. 580-591.
2. Pio-Lopez, L. and M. Levin, *Aging as a loss of morphostatic information: A developmental bioelectricity perspective.* Ageing Research Reviews, 2024. **97**: p. 102310.
3. Freitas, A.A. and J.P. de Magalhães, *A review and appraisal of the DNA damage theory of ageing.* Mutat Res, 2011. **728**(1-2): p. 12-22.
4. Gladyshev, V.N., et al., *Molecular damage in aging.* Nature Aging, 2021. **1**(12): p. 1096-1106.
5. Kirkwood, T.B. and S. Melov, *On the programmed/non-programmed nature of ageing within the life history.* Current Biology, 2011. **21**(18): p. R701-R707.
6. Trubitsyn, A.G., *The Mechanism of Programmed Aging: The Way to Create a Real Remedy for Senescence.* Curr Aging Sci, 2020. **13**(1): p. 31-41.
7. Tenchov, R., et al., *Antiaging Strategies and Remedies: A Landscape of Research Progress and Promise.* ACS Chemical Neuroscience, 2024. **15**(3): p. 408-446.
8. Lu, Y.R., X. Tian, and D.A. Sinclair, *The Information Theory of Aging.* Nature Aging, 2023. **3**(12): p. 1486-1499.
9. Rubin, H., *Ordered heterogeneity and its decline in cancer and aging.* Advances in cancer research, 2007. **98**: p. 117-47.
10. Rubin, H., *What keeps cells in tissues behaving normally in the face of myriad mutations?* BioEssays, 2006. **28**(5): p. 515-24.
11. Rubin, H., *Cellular epigenetics: control of the size, shape, and spatial distribution of transformed foci by interactions between the transformed and nontransformed cells.* Proc Natl Acad Sci U S A, 1994. **91**(3): p. 1039-43.
12. Chow, M., A. Yao, and H. Rubin, *Cellular epigenetics: topochronology of progressive "spontaneous" transformation of cells under growth constraint.* Proc Natl Acad Sci U S A, 1994. **91**(2): p. 599-603.
13. Rubin, H., *Cellular epigenetics: effects of passage history on competence of cells for "spontaneous" transformation.* Proc Natl Acad Sci U S A, 1993. **90**(22): p. 10715-9.
14. Fields, C. and M. Levin, *Competency in Navigating Arbitrary Spaces as an Invariant for Analyzing Cognition in Diverse Embodiments.* Entropy (Basel), 2022. **24**(6).
15. Pezzulo, G. and M. Levin, *Re-membering the body: applications of computational neuroscience to the top-down control of regeneration of limbs and other complex organs.* Integr Biol (Camb), 2015. **7**(12): p. 1487-517.
16. Levin, M., *Bioelectric signaling: Reprogrammable circuits underlying embryogenesis, regeneration, and cancer.* Cell, 2021. **184**(4): p. 1971-1989.
17. Bates, E., *Ion Channels in Development and Cancer.* Annu Rev Cell Dev Biol, 2015. **31**: p. 231-47.
18. Harris, M.P., *Bioelectric signaling as a unique regulator of development and regeneration.* Development, 2021. **148**(10).
19. Sundelacruz, S., M. Levin, and D.L. Kaplan, *Role of membrane potential in the regulation of cell proliferation and differentiation.* Stem Cell Rev Rep, 2009. **5**(3): p. 231-46.
20. Blackiston, D.J., K.A. McLaughlin, and M. Levin, *Bioelectric controls of cell proliferation: ion channels, membrane voltage and the cell cycle.* Cell Cycle, 2009. **8**(21): p. 3519-28.
21. Pai, V.P., et al., *Genome-wide analysis reveals conserved transcriptional responses downstream of resting potential change in Xenopus embryos, axolotl regeneration, and human mesenchymal cell differentiation.* Regeneration (Oxf), 2016. **3**(1): p. 3-25.
22. Lang, F., et al., *Ion channels in cell proliferation and apoptotic cell death.* The Journal of membrane biology, 2005. **205**: p. 147-157.

23. Schwab, A. and C. Stock, *Ion channels and transporters in tumour cell migration and invasion*. Philosophical Transactions of the Royal Society B: Biological Sciences, 2014. **369**(1638): p. 20130102.
24. Chen, L., F. Hassani Nia, and T. Stauber, *Ion Channels and Transporters in Muscle Cell Differentiation*. International Journal of Molecular Sciences, 2021. **22**(24): p. 13615.
25. Li, B., et al., *Nuclear BK channels regulate gene expression via the control of nuclear calcium signaling*. Nature neuroscience, 2014. **17**(8): p. 1055-1063.
26. Galva, C., P. Artigas, and C. Gatto, *Nuclear Na+/K+-ATPase plays an active role in nucleoplasmic Ca2+ homeostasis*. J Cell Sci, 2012. **125**(24): p. 6137-6147.
27. Chen, Y., et al., *Functional KV10.1 Channels Localize to the Inner Nuclear Membrane*. PLOS ONE, 2011. **6**(5): p. e19257.
28. Mazzanti, M., J.O. Bustamante, and H. Oberleithner, *Electrical dimension of the nuclear envelope*. Physiological Reviews, 2001. **81**(1): p. 1-19.
29. Mathews, J. and M. Levin, *Gap junctional signaling in pattern regulation: Physiological network connectivity instructs growth and form*. Dev Neurobiol, 2017. **77**(5): p. 643-673.
30. Wang, E.T. and M. Zhao, *Regulation of tissue repair and regeneration by electric fields*. Chin J Traumatol, 2010. **13**(1): p. 55-61.
31. Zhao, M., *Electrical fields in wound healing-An overriding signal that directs cell migration*. Semin Cell Dev Biol, 2009. **20**(6): p. 674-82.
32. George, L.F. and E.A. Bates, *Mechanisms Underlying Influence of Bioelectricity in Development*. Front Cell Dev Biol, 2022. **10**: p. 772230.
33. Levin, M., *Molecular bioelectricity: how endogenous voltage potentials control cell behavior and instruct pattern regulation in vivo*. Molecular biology of the cell, 2014. **25**(24): p. 3835-50.
34. Levin, M. and C.J. Martyniuk, *The bioelectric code: An ancient computational medium for dynamic control of growth and form*. Biosystems, 2018. **164**: p. 76-93.
35. Pai, V.P. and M. Levin, *HCN2 channel-induced rescue of brain, eye, heart and gut teratogenesis caused by nicotine, ethanol and aberrant notch signalling*. Wound Repair Regen, 2022.
36. Pai, V.P., et al., *HCN2 Rescues brain defects by enforcing endogenous voltage pre-patterns*. Nature Communications, 2018. **9**(1): p. 998.
37. Pai, V.P., et al., *Endogenous Gradients of Resting Potential Instructively Pattern Embryonic Neural Tissue via Notch Signaling and Regulation of Proliferation*. The Journal of Neuroscience, 2015. **35**(10): p. 4366-85.
38. Pai, V.P., et al., *Local and long-range endogenous resting potential gradients antagonistically regulate apoptosis and proliferation in the embryonic CNS*. The International journal of developmental biology, 2015. **59**(7-9): p. 327-340.
39. Rubin, H., M. Chow, and A. Yao, *Cellular aging, destabilization, and cancer*. Proc Natl Acad Sci U S A, 1996. **93**(5): p. 1825-30.
40. Lobikin, M., et al., *Resting potential, oncogene-induced tumorigenesis, and metastasis: the bioelectric basis of cancer in vivo*. Physical Biology, 2012. **9**(6): p. 065002.
41. Chernet, B.T. and M. Levin, *Endogenous Voltage Potentials and the Microenvironment: Bioelectric Signals that Reveal, Induce and Normalize Cancer*. Journal of clinical & experimental oncology, 2013. **Suppl 1**.
42. Chernet, B.T. and M. Levin, *Transmembrane voltage potential is an essential cellular parameter for the detection and control of tumor development in a Xenopus model*. Disease models & mechanisms, 2013. **6**(3): p. 595-607.

43. Prevarskaya, N., R. Skryma, and Y. Shuba, *Ion Channels in Cancer: Are Cancer Hallmarks Oncochannelopathies?* Physiol Rev, 2018. **98**(2): p. 559-621.
44. Foust, A.J., et al., *Voltage-Sensitive Optical Probes for Measuring Cell Membrane Potentials: An Update and Applications to "Nonexcitable" Cells.* Bioelectricity, 2023. **5**(4): p. 250-265.
45. Payne, S.L., M. Levin, and M.J. Oudin, *Bioelectric Control of Metastasis in Solid Tumors.* Bioelectricity, 2019. **1**(3): p. 114-130.
46. Levin, M., J. Selberg, and M. Rolandi, *Endogenous Bioelectrics in Development, Cancer, and Regeneration: Drugs and Bioelectronic Devices as Electroceuticals for Regenerative Medicine.* iScience, 2019. **22**: p. 519-533.
47. McLaughlin, K.A. and M. Levin, *Bioelectric signaling in regeneration: Mechanisms of ionic controls of growth and form.* Dev Biol, 2018. **433**(2): p. 177-189.
48. Pchelintseva, E. and M.B.A. Djamgoz, *Mesenchymal stem cell differentiation: Control by calcium-activated potassium channels.* J Cell Physiol, 2018. **233**(5): p. 3755-3768.
49. Sundelacruz, S., M. Levin, and D.L. Kaplan, *Depolarization alters phenotype, maintains plasticity of predifferentiated mesenchymal stem cells.* Tissue engineering. Part A, 2013. **19**(17-18): p. 1889-908.
50. Sundelacruz, S., et al., *Membrane Potential Depolarization Alters Calcium Flux and Phosphate Signaling During Osteogenic Differentiation of Human Mesenchymal Stem Cells.* Bioelectricity, 2019. **1**(1): p. 56-66.
51. Sundelacruz, S., M. Levin, and D.L. Kaplan, *Comparison of the depolarization response of human mesenchymal stem cells from different donors.* Sci Rep, 2015. **5**: p. 18279.
52. Bhuyan, A.K., A. Varshney, and M.K. Mathew, *Resting membrane potential as a marker of apoptosis: studies on Xenopus oocytes microinjected with cytochrome c.* Cell Death & Differentiation, 2001. **8**(1): p. 63-69.
53. Nelson, M.T. and J.M. Quayle, *Physiological roles and properties of potassium channels in arterial smooth muscle.* Am J Physiol, 1995. **268**(4 Pt 1): p. C799-822.
54. Rühl, P., et al., *Monitoring of compound resting membrane potentials of cell cultures with ratiometric genetically encoded voltage indicators.* Communications Biology, 2021. **4**(1): p. 1164.
55. McMillen, P. and M. Levin, *Optical Estimation of Bioelectric Patterns in Living Embryos.* Methods Mol Biol, 2024. **2745**: p. 91-102.
56. Kirk, M.J., B.K. Raliski, and E.W. Miller, *Monitoring neuronal activity with voltage-sensitive fluorophores.* Methods Enzymol, 2020. **640**: p. 185-204.
57. Li, M., et al., *PPP3R1 Promotes MSCs Senescence by Inducing Plasma Membrane Depolarization and Increasing Ca2+ Influx.* International Journal of Molecular Sciences, 2023. **24**(5): p. 4421.
58. Chen, A., et al., *mTORC1 induces plasma membrane depolarization and promotes preosteoblast senescence by regulating the sodium channel Scn1a.* Bone Research, 2022. **10**(1).
59. Warnier, M., et al., *The <scp>SCN</scp>9A channel and plasma membrane depolarization promote cellular senescence through Rb pathway.* Aging Cell, 2018. **17**(3): p. e12736.
60. Whited, J.L. and M. Levin, *Bioelectrical controls of morphogenesis: from ancient mechanisms of cell coordination to biomedical opportunities.* Curr Opin Genet Dev, 2019. **57**: p. 61-69.
61. Vandenberg, L.N., R.D. Morrie, and D.S. Adams, *V-ATPase-dependent ectodermal voltage and pH regionalization are required for craniofacial morphogenesis.* Dev Dyn, 2011. **240**(8): p. 1889-904.

62. Park, S.C., et al., *What matters in aging is signaling for responsiveness.* Pharmacol Ther, 2023. **252**: p. 108560.
63. Eckert, R.L., et al., *Keratinocyte survival, differentiation, and death: many roads lead to mitogen-activated protein kinase.* J Investig Dermatol Symp Proc, 2002. **7**(1): p. 36-40.
64. Gruber, F., et al., *Cell aging and cellular senescence in skin aging — Recent advances in fibroblast and keratinocyte biology.* Experimental Gerontology, 2020. **130**: p. 110780.
65. Krzystyniak, A., et al., *Fiji-Based Tool for Rapid and Unbiased Analysis of SA-β-Gal Activity in Cultured Cells.* Biomolecules, 2023. **13**(2): p. 362.
66. Rutledge, R.G., *A Java Program for LRE-Based Real-Time qPCR that Enables Large-Scale Absolute Quantification.* PLoS ONE, 2011. **6**(3): p. e17636.
67. Huang, Y.L., A.S. Walker, and E.W. Miller, *A Photostable Silicon Rhodamine Platform for Optical Voltage Sensing.* J Am Chem Soc, 2015. **137**(33): p. 10767-76.
68. Walker, A.S., et al., *Optical Spike Detection and Connectivity Analysis With a Far-Red Voltage-Sensitive Fluorophore Reveals Changes to Network Connectivity in Development and Disease.* Frontiers in Neuroscience, 2021. **15**.
69. McMillen, P. and M. Levin, *Optical Estimation of Bioelectric Patterns in Living Embryos*. 2024, Springer US. p. 91-102.
70. Lazzari-Dean, J.R., A.M.M. Gest, and E.W. Miller, *Optical estimation of absolute membrane potential using fluorescence lifetime imaging.* eLife, 2019. **8**: p. e44522.
71. Liu, P. and E.W. Miller, *Electrophysiology, Unplugged: Imaging Membrane Potential with Fluorescent Indicators.* Accounts of Chemical Research, 2020. **53**(1): p. 11-19.
72. Lapak, K.M. and C.E. Burd, *The Molecular Balancing Act of p16INK4a in Cancer and Aging.* Molecular Cancer Research, 2014. **12**(2): p. 167-183.
73. Hartmann, C., et al., *Systematic estimation of biological age of in vitro cell culture systems by an age-associated marker panel.* Frontiers in Aging, 2023. **4**.
74. Shaban, H.A. and S.M. Gasser, *Dynamic 3D genome reorganization during senescence: defining cell states through chromatin.* Cell Death & Differentiation, 2025. **32**(1): p. 9-15.
75. Djamgoz, M.B.A., *Electrical excitability of cancer cells-CELEX model updated.* Cancer Metastasis Rev, 2024. **43**(4): p. 1579-1591.
76. Balasubramanian, S., et al., *Electroceuticals: emerging applications beyond the nervous system and excitable tissues.* Trends Pharmacol Sci, 2024. **45**(5): p. 391-394.
77. Churchill, C.D.M., et al., *EDEn – Electroceutical Design Environment: An Ion Channel Database with Small Molecule Modulators and Tissue Expression Information.* iScience, 2018. **11**: p. 42-56.
78. Cao, C., et al., *ATP-sensitive potassium channel: A novel target for protection against UV-induced human skin cell damage.* Journal of Cellular Physiology, 2007. **212**(1): p. 252-263.
79. Weiss, I. and J. Bohrmann, *Electrochemical patterns during Drosophila oogenesis: ion-transport mechanisms generate stage-specific gradients of pH and membrane potential in the follicle-cell epithelium.* Bmc Developmental Biology, 2019. **19**(1): p. 12.
80. Durant, F., et al., *Long-Term, Stochastic Editing of Regenerative Anatomy via Targeting Endogenous Bioelectric Gradients.* Biophysical Journal, 2017. **112**(10): p. 2231-2243.
81. Schmal, C., et al., *Moran's I quantifies spatio-temporal pattern formation in neural imaging data.* Bioinformatics, 2017. **33**(19): p. 3072-3079.
82. Venkatachalam, K., *Regulation of Aging and Longevity by Ion Channels and Transporters.* Cells, 2022. **11**(7): p. 1180.
83. Wiley, C.D., et al., *Analysis of individual cells identifies cell-to-cell variability following induction of cellular senescence.* Aging Cell, 2017. **16**(5): p. 1043-1050.

84. Matsuda, T., et al., *Decreased response to epidermal growth factor during cellular senescence in cultured human microvascular endothelial cells.* Journal of Cellular Physiology, 1992. **150**(3): p. 510-516.
85. Palmer, A.K., et al., *Targeting senescent cells alleviates obesity-induced metabolic dysfunction.* Aging Cell, 2019. **18**(3): p. e12950.
86. Marrella, V., A. Facoetti, and B. Cassani, *Cellular Senescence in Immunity against Infections.* International Journal of Molecular Sciences, 2022. **23**(19): p. 11845.
87. Dardevet, D., et al., *Leucine: a key amino acid in ageing-associated sarcopenia?* Nutrition Research Reviews, 2003. **16**(01): p. 61.
88. Qiu, Z., et al., *Detection of differentially expressed genes in spatial transcriptomics data by spatial analysis of spatial transcriptomics: A novel method based on spatial statistics.* Frontiers in Neuroscience, 2022. **16**.
89. Pai, V.P., et al., *Endogenous gradients of resting potential instructively pattern embryonic neural tissue via Notch signaling and regulation of proliferation.* J Neurosci, 2015. **35**(10): p. 4366-85.
90. Schotthofer, S.K. and J. Bohrmann, *Analysing bioelectrical phenomena in the Drosophila ovary with genetic tools: tissue-specific expression of sensors for membrane potential and intracellular pH, and RNAi-knockdown of mechanisms involved in ion exchange.* BMC Dev Biol, 2020. **20**(1): p. 15.
91. Weiss, I. and J. Bohrmann, *Electrochemical gradients are involved in regulating cytoskeletal patterns during epithelial morphogenesis in the Drosophila ovary.* BMC Dev Biol, 2019. **19**(1): p. 22.
92. Telfer, W., R. Woodruff, and E. Huebner, *Electrical polarity and cellular differentiation in meroistic ovaries.* American Zoologist, 1981. **21**: p. 675-686.
93. Woodruff, R. and W. Telfer, *Electrophoresis of proteins in intercellular bridges.* Nature, 1980. **286**(5768): p. 84-6.
94. Jaffe, L. and R. Woodruff, *Large electrical currents traverse developing Cecropia follicles.* Proceedings of the National Academy of Sciences of the United States of America, 1979. **76**(3): p. 1328-1332.
95. Woodruff, R. and W. Telfer, *Electrical properties of ovarian cells linked by intercellular bridges.* Annals of the New York Academy of Sciences, 1974. **238**: p. 408-19.
96. Cervera, J., S. Meseguer, and S. Mafe, *Intercellular Connectivity and Multicellular Bioelectric Oscillations in Nonexcitable Cells: A Biophysical Model.* ACS Omega, 2018. **3**(10): p. 13567-13575.
97. Cervera, J., et al., *From non-excitable single-cell to multicellular bioelectrical states supported by ion channels and gap junction proteins: Electrical potentials as distributed controllers.* Prog Biophys Mol Biol, 2019. **149**: p. 39-53.
98. Cervera, J., et al., *Synchronization of Bioelectric Oscillations in Networks of Nonexcitable Cells: From Single-Cell to Multicellular States.* J Phys Chem B, 2019. **123**(18): p. 3924-3934.
99. Pietak, A. and M. Levin, *Bioelectric gene and reaction networks: computational modelling of genetic, biochemical and bioelectrical dynamics in pattern regulation.* J R Soc Interface, 2017. **14**(134).
100. Pietak, A. and M. Levin, *Exploring Instructive Physiological Signaling with the Bioelectric Tissue Simulation Engine (BETSE).* Frontiers in Bioengineering and Biotechnology, 2016. **4**: p. 55.
101. Mathews, J., et al., *Ion Channel Drugs Suppress Cancer Phenotype in NG108-15 and U87 Cells: Toward Novel Electroceuticals for Glioblastoma.* Cancers, 2022. **14**(6): p. 1499.

102. Stevenson, D., et al., *Relationship between cell membrane potential and natural killer cell cytolysis in human hepatocellular carcinoma cells.* Cancer Res, 1989. **49**(17): p. 4842-5.
103. Srivastava, P., et al., *A Meta-Analysis of Bioelectric Data in Cancer, Embryogenesis, and Regeneration.* Bioelectricity, 2020. **in press**(1): p. 42-67.
104. Xie, H.Q. and V.W. Hu, *Modulation of gap junctions in senescent endothelial cells.* Exp Cell Res, 1994. **214**(1): p. 172-6.
105. Pio-Lopez, L. and M. Levin, *Aging as a loss of morphostatic information: A developmental bioelectricity perspective.* Ageing Res Rev, 2024. **97**: p. 102310.

Figure Legends:

Figure 1 – Aged Human Epidermal Keratinocytes Depolarize, Exhibit Increased Inter- and Reduced Intra-culture V_{mem} Heterogeneity. Human epidermal keratinocytes were cultured onto flat-bottom 96-well plate 24-hours prior to imaging. Cells were loaded with 600 nM BeRST in Keratinocyte Media for 30-minutes in humidified incubator at 37oC and 5% CO2, then washed twice with PBS and kept in fresh Keratinocyte Media for imaging with the Leica SP8 Confocal microscope. (A) Human epidermal keratinocytes became significantly depolarized at day 40 and 50 (n=6 biological replicates, $p<0.05$ and $p<0.001$, respectively)). (B) The calculated standard deviation of each biological replicate shows increased variability between replicates. (C) The average standard deviation within each biological i.e. within a single dish was calculated by averaging the standard deviation in each age group. This analysis revealed that variability within a single cell culture significantly decreases with age. (D) Representative FLIM Images of BeRST stained Keratinocytes.

Figure 2 – Aging Biomarkers Significantly Increases 50-day Keratinocyte Cultures. Human epidermal keratinocytes thawed 7-days prior were plated in 6-well plate and 96-well for p16 mRNA expression, and senescence associated β-galactosidase and Chromatin condensation level characterization, respectively. (A) Results from RT-qPCR were normalized to 10-day old cells and revealed a two-fold increase in p16 expression in 50-day old cells ($p<0.05$, n=4 biological replicates). (B) Inverse images of β-galactosidase-stained Keratinocyte were generated in ImageJ, then the integrated density of the stained areas was calculated and divided by the number of nuclei in the image to calculate the 'Integrated Density of βGal Signal Per Cell'. Results revealed 9. 8-fold increase in 50-day old cells compared to 10-day old cells ($p<0.0001$, n=6 biological replicates). Analysis of chromatin condensation levels revealed 50-day old cells with the highest degree of compaction. (C) Representative images of (i) β-galactosidase-stained Keratinocyte and (ii) CCP images showing 50-day old cells with highest number of intra-nuclear edges.

Figure 3 – Senescent Human Epidermal Keratinocytes Exhibit Reduced Responsiveness and Resilience. Human Epidermal Keratinocytes cultured in 96-well plate were stained with 600 nM BeRST and kept in a humidified incubator (37ºC; 5% CO_2) for 30-minutes and washed twice with PBS prior to imaging with the Leica SP8 Confocal Microscope. Keratinocytes were initially imaged to establish pre-treatment baseline, then given fresh media containing 10 μM Pinacidil just prior to imaging. Percentage change in the Fluorescence Lifetime of BeRST was calculated by subtracting and dividing post-treatment values by pretreatment average value. (A) Treatment with Pinacidil revealed significant increase in responsiveness at 30-days ($p<0.05$, n=3 biological replicates), and significant decrease in responsiveness at 40 and 50-days ($p< 0.0001$; n=8). (B) The timeseries variability of 50-day old cells, measured by the standard deviation, was significantly larger than younger cells. (C) Average Timeseries of each age group shows that younger cells (Day 10 – 40) hyperpolarize when exposed to pinacidil and exhibit a relatively stable oscillation of V_{mem}. However, 50-day old cells immediately undergo depolarization followed by hyperpolarization and a return towards depolarization.

Figure 4 – Spatial Organization and Clustering is Significantly Reduced in Older Keratinocytes**.** Human Epidermal Keratinocytes were stained with the Vmem dye, Vf2.1 (50 nM) for 30-minutes in a humidified incubator at 37ºC and 5% CO_2, then washed twice with PBS and given fresh keratinocyte media. Fluorescence Lifetime Imaging was performed with the Leica SP8 Confocal microscope. The collected FLIM images were fitted with biexponential decay curve in the Leica suit, thresholded to remove background, and exported as '.Tif' files for further analysis. Using a 15 x 15 pixel ROI was used to scan the image and generate an excel file containing 'X', 'Y', and 'Lifetime' for rois above 100% 'ON' pixels'. To determine the appropriate 'k' value, i.e. number of clusters, for the Moran's I calculation, we initially ran an elbow test to trial k values from 1 – 10 and determined the elbow of the curve to be at k=3. To control

for differences in cell number, we subsampled our data (1000 cells) with 10 iterations which was then averaged. (A) Results revealed significant reduction in Moran's I in 40- ($p=0.0011$, n=7 biological replicates) and 50-day ($p=0.0005$, n=10 biological replicates) old cells compared to 10-day old cells (n=10 biological replicates). (B) Moran's I scatter plots generated by plotting the Lifetime against spatial lag Lifetime shows localization of points in the top right corner of the quadrant, revealing a positive spatial correlation. This correlation appeared strongest in the 10-day old cells ($r^2=0.58$) and significantly reduced by day 40 and 50 ($r^2=0.02$, and $r^2=0.08$, respectively). C) Representative images mapping distribution of local Moran's I reveal significantly more distinct clustering in younger cells, and a progressive decrease in size and distribution with age. Red points represents distinct clusters relative to the bulk population, whereas blue points represents non-significant clustering. (D) Representative BeRST FLIM images.

Figure 5 – Hyperpolarizing Reduces while Depolarizing Keratinocytes Increases Senescence Phenotypes. Keratinocytes 30-days old were either cultured in control mediate, media containing 10 μM Pinacidil, or 25 mM potassium gluconate for 6 days. Media was replaced every second day; after the sixth day, all groups were given fresh control media. On day 8, cells were stained with BeRST and Hoechst 33432, then imaged using the Leica SP8 confocal microscope. (A) Treatment with Pinacidil (10 μM) resulted in almost three-fold increase in cell number ($p<0.0001$, n=18 biological replicates) compared to the control group. Conversely, treatment with potassium gluconate resulted in significant reduction in cel number ($p<0.05$, n=24 biological replicates) . (B) The βGal/nuclei signal significantly increased in cells treated with potassium gluconate (n=6 biological replicates) compared to control cells ($p<0.001$, n=12 biological replicates). Pinacidil treated cells did not exhibit a significant reduction when compared to control group; however, compared to the potassium gluconate group, pinacidil treated cells had a significantly lower βGal/nuc signal. (C) Chromatin condensation levels of depolarized was significantly higher, while hyperpolarized cells exhibited significantly reduced compaction. (D) Representative images of (i) Hoechst nuclei, (ii) processed images of Hoechst nuclei for CCP computation, and (iii) βGal levels.

Figure 6 – Hyperpolarizing Keratinocytes Maintains Cellular Responsiveness. Keratinocytes at 30-days of culture were grown for an additional 6 days in either control media, media containing Pinacidil or potassium gluconate (+ 25 mM). They were then given fresh control media and grown for another two days, then stained with 600 nM BeRST and 1 μM Hoechst 33432 prior to imaging. Keratinocytes (A) The percentage change in BeRST lifetime was significantly higher in Pinacidil treated cells compared to control ($p<0.01$, control n=4 biological replicates, Pinacidil n=3 biological replicates). Treatment with potassium gluconate appeared to decrease the level of responsiveness; however, this was not significantly different than control cells. (B) Average timeseries of each group reveals control cells appeared to oscillate near 0%, whereas, potassium gluconate treated cells, progressively became hyperpolarized. Notably, pinacidil treated cells progressively depolarized over time.

Figure 7 – Depolarization of Keratinocytes Leads to Loss of Spatial Organization and Clustering. Keratinocytes at 30-days of culture were grown for an additional 6 days in either control media, media containing Pinacidil or potassium gluconate (+ 25 mM). They were then given fresh control media and grown for another two days, then immediately prior to imaging, cells were stained with 50 nM VF2.1 and 1 μM Hoechst 33342 for 30-minutes in a humidified incubator at 37ºC and 5% CO_2, washed twice with PBS and then given fresh keratinocyte media. Fluorescence Lifetime Imaging was performed with the Leica SP8 Confocal microscope. The collected FLIM images were fitted with biexponential decay curve in the Leica suit, thresholded to remove background, and exported as '.Tif' files for further analysis. Using a 15 x 15 pixels ROI was used to scan the image and generate an excel file containing 'X', 'Y', and 'Lifetime' for ROIs above 100% 'ON' pixels. To determine the appropriate 'k' value, i.e. number of clusters, for the Moran's I calculation, we initially ran an elbow test to trial k values from 1 – 10 and determined the elbow of the curve to be at k=3. To control for differences in cell number, we subsampled our data (1000 cells)

with 10 iterations which was then averaged. (A) Pre-treatment with Pinacidil did not result in a significant change; however, potassium gluconate treatment significantly reduced Moran's I from 0.63 to 0.26 ($p<0.01$, control n=4 biological replicates, potassium gluconate n=4 biological replicates). (B-i) Scatter plot of Lifetime vs spatial lag Lifetime also revealed a more random distribution of points, consistent with reduced spatial autocorrelation. (C) Local Moran computation shows reduction in size and distribution of distinct clusters in potassium gluconate pre-treated cells. (D) representative images of VF2.1 stained cells showing corresponding clusters.

Supplementary Figure 1 – Control Dye VF2.0 Reveals Concentration Dependent Spatial Artifacts. Keratinocytes at 20-days of culture were stained with 600 nM or 50 nM VF2.0 for 30-minutes in a humidified incubator at 37ºC and 5% CO_2, washed twice with PBS and then given fresh keratinocyte media. Fluorescence Lifetime Imaging was performed with the Leica SP8 Confocal microscope. The collected FLIM images were fitted with biexponential decay curve in the Leica suit, thresholded to remove background, and exported as '.Tif' files for further analysis. Using a 15 x 15 pixels ROI was used to scan the image and generate an excel file containing 'X', 'Y', and 'Lifetime' for rois above 100% 'ON' pixels. To control for differences in cell number, we subsampled our data (1000 cells) with 10 iterations which was then averaged. (A) Violin plot showing high spatial Moran's I of 0.50 in keratinocytes stained with 600 nM; however, reducing concentration to 50 nM resulted in a Moran's I of 0.04 ($p< 0.001$, n= 3 replicates). (B) Representative images showing artifactual clustering.

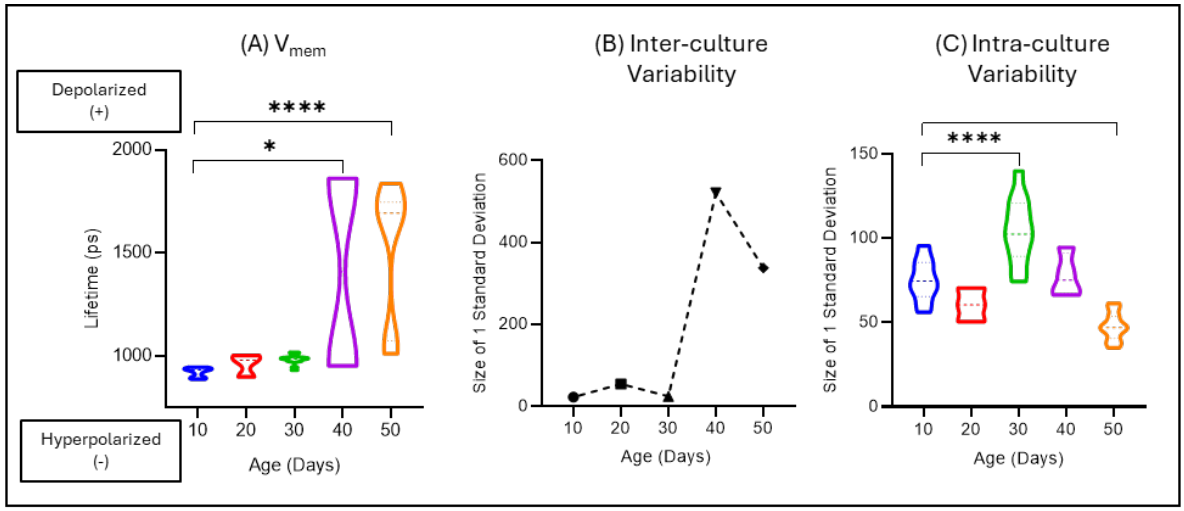

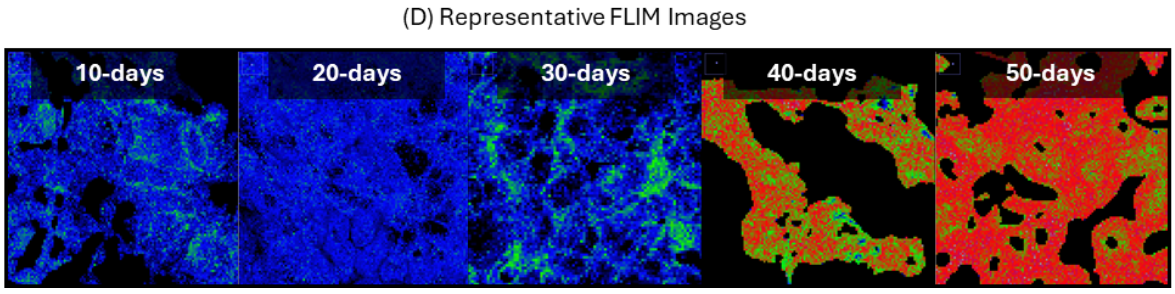

Figure 1 – Aged Human Epidermal Keratinocytes Depolarize, Exhibit Increased Inter- and Reduced Intra-culture V_{mem} Heterogeneity. Human epidermal keratinocytes were cultured onto flat-bottom 96-well plate 24-hours prior to imaging. Cells were loaded with 600 nM BeRST in Keratinocyte Media for 30-minutes in humidified incubator at 37°C and 5% CO_2, then washed twice with PBS and kept in fresh Keratinocyte Media for imaging with the Leica SP8 Confocal microscope. (A) Human epidermal keratinocytes became significantly depolarized at day 40 and 50 (n=6 biological replicates, $p<0.05$ and $p<0.001$, respectively)). (B) The calculated standard deviation of each biological replicate shows increased variability between replicates. (C) The average standard deviation within each biological i.e. within a single dish was calculated by averaging the standard deviation in each age group. This analysis revealed that variability within a single cell culture significantly decreases with age. (D) Representative FLIM Images of BeRST stained Keratinocytes.

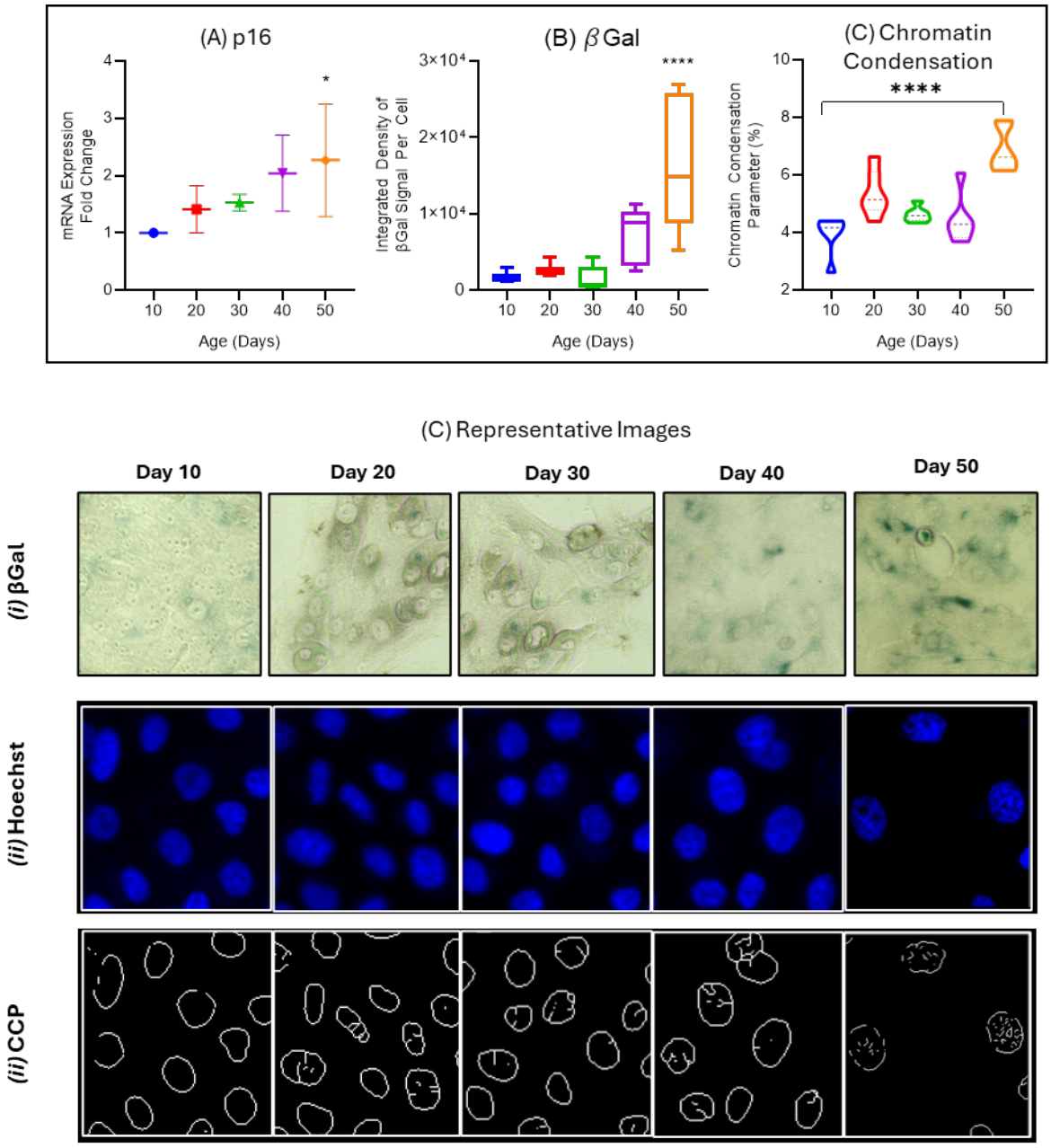

Figure 2 – Aging Biomarkers Significantly Increases 50-day Keratinocyte Cultures. Human epidermal keratinocytes thawed 7-days prior were plated in 6-well plate and 96-well for p16 mRNA expression, and senescence associated b-galactosidase and Chromatin condensation level characterization, respectively. (A) Results from RT-qPCR were normalized to 10-day old cells and revealed a two-fold increase in p16 expression in 50-day old cells ($p<0.05$, n=4 biological replicates). (B) Inverse images of β-galactosidase-stained Keratinocyte were generated in ImageJ, then the integrated density of the stained areas was calculated and divided by the number of nuclei in the image to calculate the 'Integrated Density of βGal Signal Per Cell'. Results revealed 9. 8-fold increase in 50-day old cells compared to 10-day old cells ($p<0.0001$, n=6 biological replicates). Analysis of chromatin condensation levels revealed 50-day old cells with the highest degree of compaction. (C) Representative images of (i) β-galactosidase-stained Keratinocyte and (*ii*) CCP images showing 50-day old cells with highest number of intra-nuclear edges.

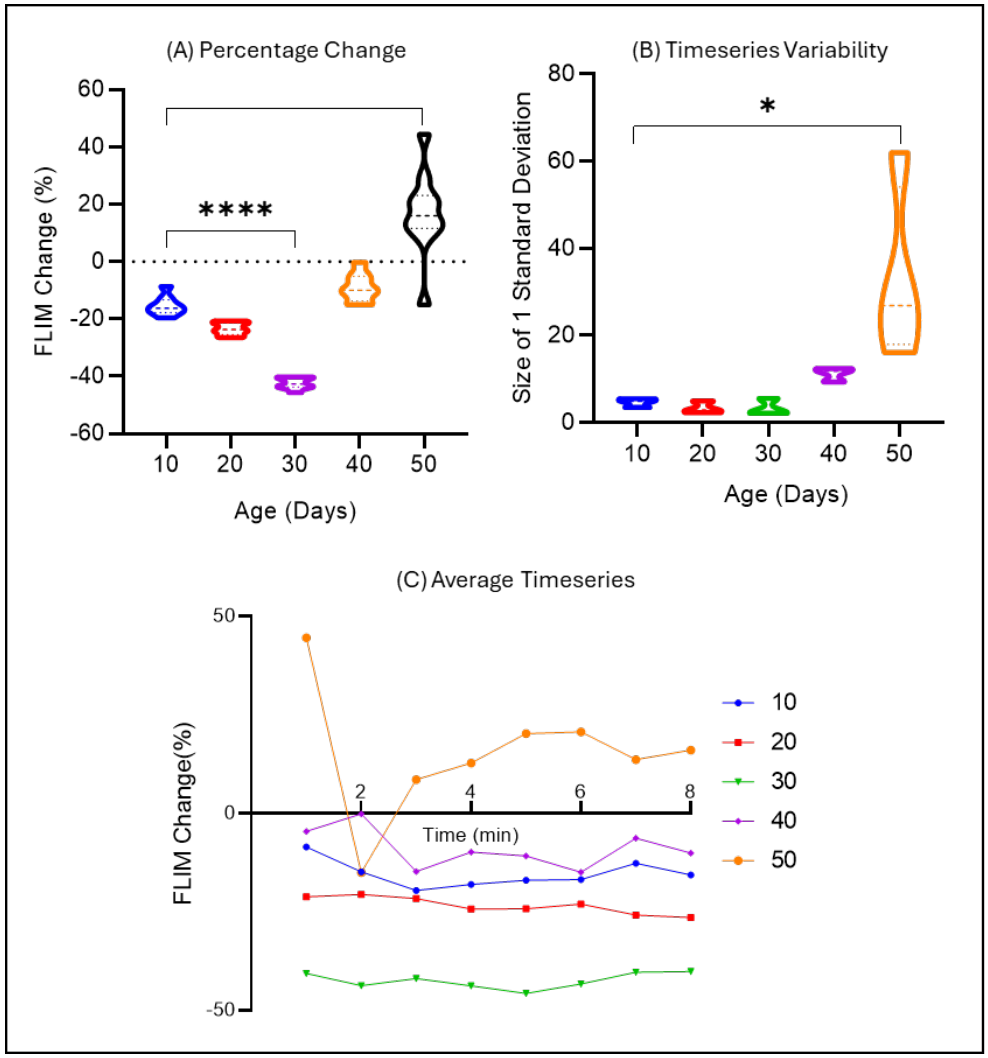

Figure 3 – Senescent Human Epidermal Keratinocytes Exhibit Reduced Responsiveness and Resilience. Human Epidermal Keratinocytes cultured in 96-well plate were stained with 600 nM BeRST and kept in a humidified incubator (37°C; 5% CO_2) for 30-minutes and washed twice with PBS prior to imaging with the Leica SP8 Confocal Microscope. Keratinocytes were initially imaged to establish pre-treatment baseline, then given fresh media containing 10 μM Pinacidil just prior to imaging. Percentage change in the Fluorescence Lifetime of BeRST was calculated by subtracting and dividing post-treatment values by pretreatment average value. (A) Treatment with Pinacidil revealed significant increase in responsiveness at 30-days ($p<0.05$, n=3 biological replicates), and significant decrease in responsiveness at 40 and 50-days ($p< 0.0001$; n=8). (B) The timeseries variability of 50-day old cells, measured by the standard deviation, was significantly larger than younger cells. (C) Average Timeseries of each age group shows that younger cells (Day 10 – 40) hyperpolarize when exposed to pinacidil and exhibit a relatively stable oscillation of V_{mem}. However, 50-day old cells immediately undergo depolarization followed by hyperpolarization and a return towards depolarization.

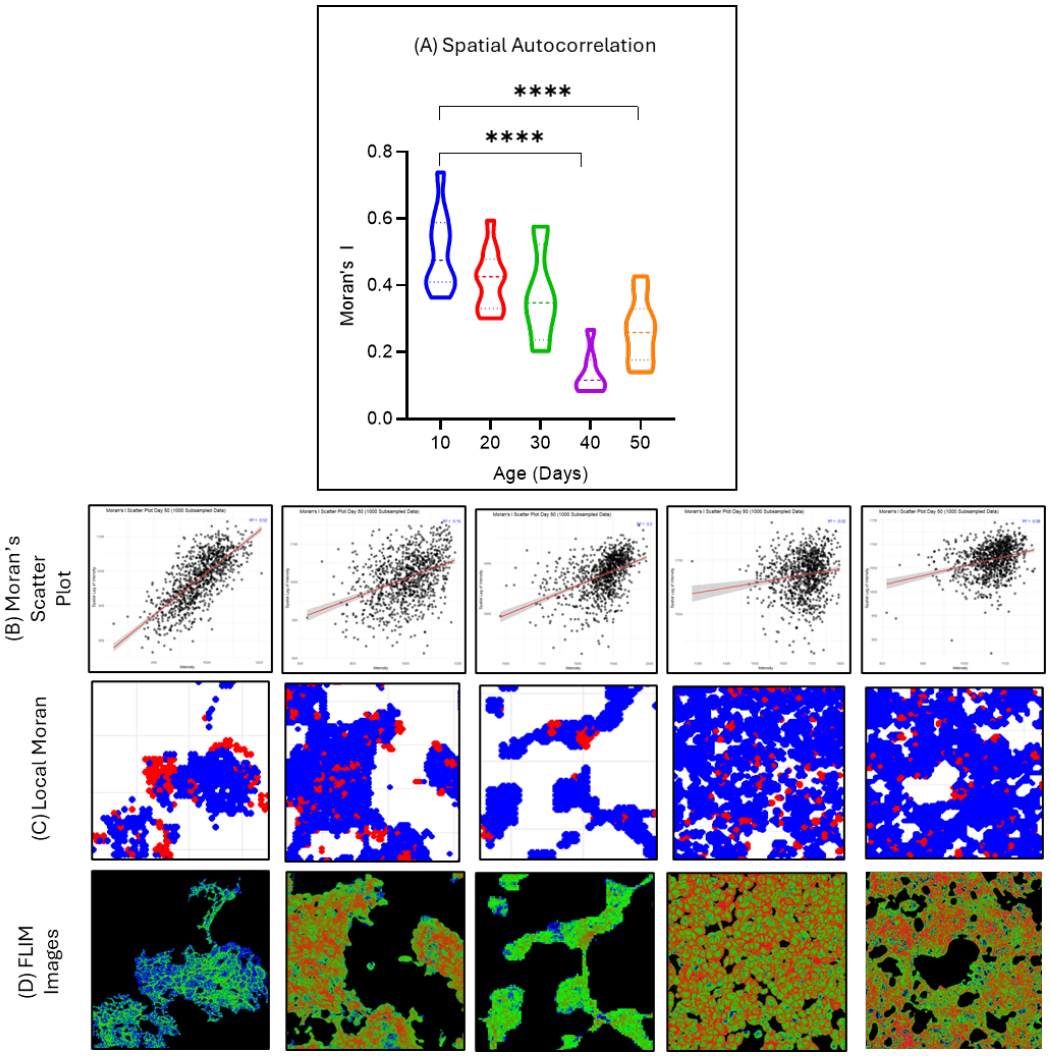

Figure 4 – Spatial Organization and Clustering is Significantly Reduced in Older Keratinocytes. Human Epidermal Keratinocytes were stained with the Vmem dye, Vf2.1 (50 nM) for 30-minutes in a humidified incubator at 37°C and 5% CO_2, then washed twice with PBS and given fresh keratinocyte media. Fluorescence Lifetime Imaging was performed with the Leica SP8 Confocal microscope. The collected FLIM images were fitted with biexponential decay curve in the Leica suit, thresholded to remove background, and exported as '.Tif' files for further analysis. Using a 15 x 15 pixel ROI was used to scan the image and generate an excel file containing 'X', 'Y', and 'Lifetime' for rois above 100% 'ON' pixels'. To determine the appropriate 'k' value, i.e. number of clusters, for the Moran's I calculation, we initially ran an elbow test to trial k values from 1 – 10 and determined the elbow of the curve to be at k=3. To control for differences in cell number, we subsampled our data (1000 cells) with 10 iterations which was then averaged. (A) Results revealed significant reduction in Moran's I in 40- (p=0.0011, n=7 biological replicates) and 50-day (p=0.0005, n=10 biological replicates) old cells compared to 10-day old cells (n=10 biological replicates). (B) Moran's I scatter plots generated by plotting the Lifetime against spatial lag Lifetime shows localization of points in the top right corner of the quadrant, revealing a positive spatial correlation. This correlation appeared strongest in the 10-day old cells (r^2=0.58) and significantly reduced by day 40 and 50 (r^2=0.02, and r^2=0.08, respectively). C) Representative images mapping distribution of local Moran's I reveal significantly more distinct clustering in younger cells, and a progressive decrease in size and distribution with age. Red points represents distinct clusters relative to the bulk population, whereas blue points represents non-significant clustering. (D) Representative BeRST FLIM images.

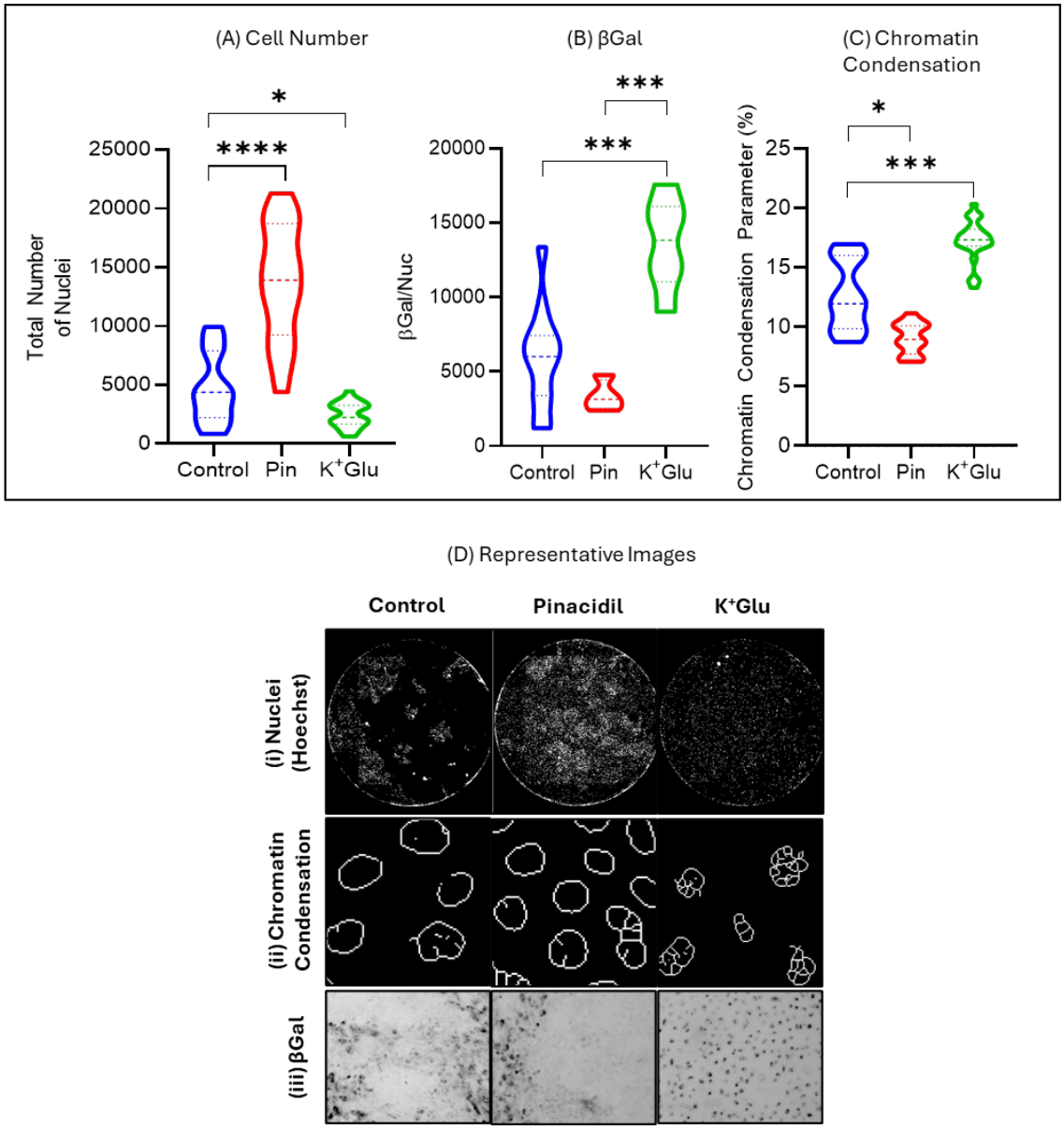

Figure 5 – Hyperpolarizing Reduces while Depolarizing Keratinocytes Increases Senescence Phenotypes. Keratinocytes 30-days old were either cultured in control mediate, media containing 10 μM Pinacidil, or 25 mM potassium gluconate for 6 days. Media was replaced every second day; after the sixth day, all groups were given fresh control media. On day 8, cells were stained with BeRST and Hoechst 33432, then imaged using the Leica SP8 confocal microscope. (A) Treatment with Pinacidil (10 μM) resulted in almost three-fold increase in cell number ($p<0.0001$, n=18 biological replicate) compared to the control group. Conversely, treatment with potassium gluconate resulted in significant reduction in cel number ($p<0.05$, n=24 biological replicate) . (B) The bGal/nuclei signal significantly increased in cells treated with potassium gluconate (n=6 biological replicate) compared to control cells ($p<0.001$, n=12 biological replicate). Pinacidil treated cells did not exhibit a significant reduction when compared to control group; however, compared to the potassium gluconate group, pinacidil treated cells had a significantly lower bGal/nuc signal. (C) Chromatin condensation levels of depolarized was significantly higher, while hyperpolarized cells exhibited significantly reduced compaction. (D) Representative images of (i) Hoechst nuclei, (ii) processed images of Hoechst nuclei for CCP computation, and (iii) βGal levels.

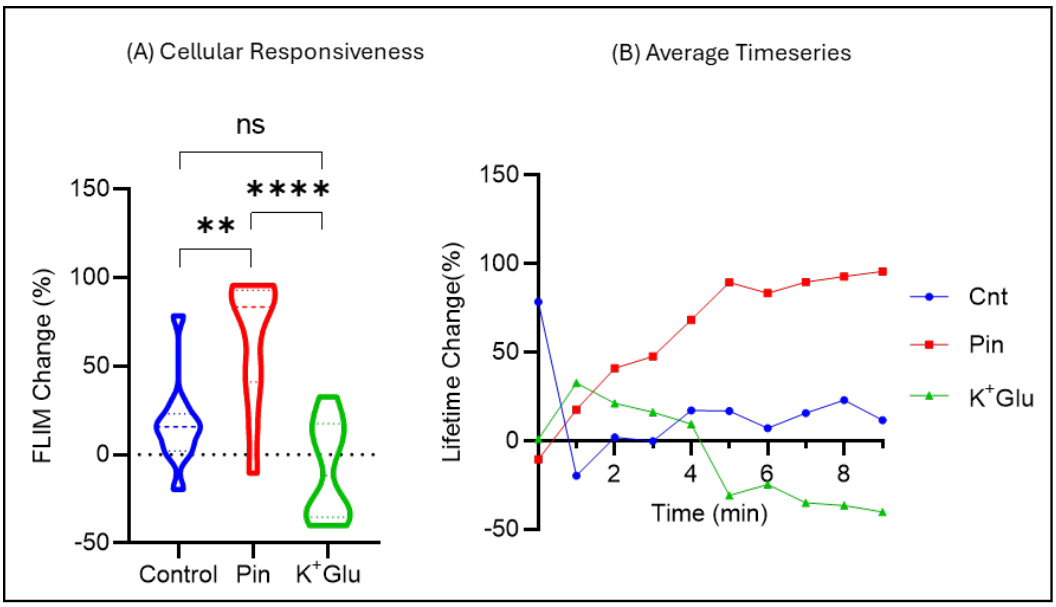

Figure 6 – Hyperpolarizing Keratinocytes Maintains Cellular Responsiveness. Keratinocytes at 30-days of culture were grown for an additional 6 days in either control media, media containing Pinacidil or potassium gluconate (+ 25 mM). They were then given fresh control media and grown for another two days, then stained with 600 nM BeRST and 1 μM Hoechst 33432 prior to imaging. Keratinocytes (A) The percentage change in BeRST lifetime was significantly higher in Pinacidil treated cells compared to control ($p<0.01$, control n=4 biological replicate, Pinacidil n=3 biological replicate). Treatment with potassium gluconate appeared to decrease the level of responsiveness; however, this was not significantly different than control cells. (B) Average timeseries of each group reveals control cells appeared to oscillate near 0%, whereas, potassium gluconate treated cells, progressively became hyperpolarized. Notably, pinacidil treated cells progressively depolarized over time.

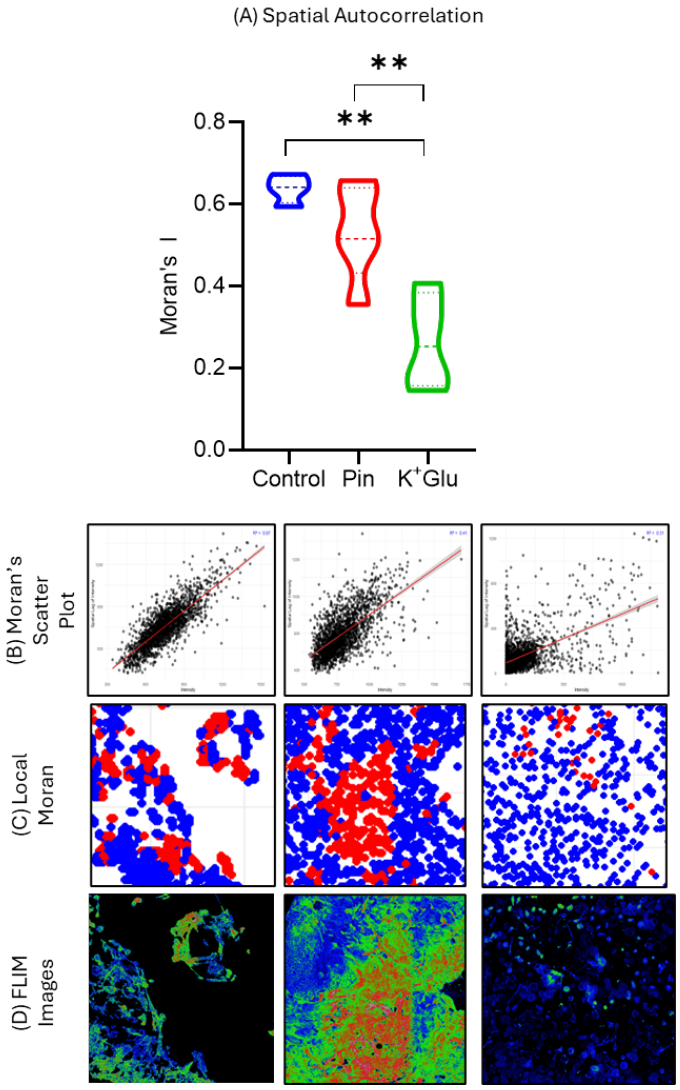

Figure 7 – Depolarization of Keratinocytes Leads to Loss of Spatial Organization and Clustering. Keratinocytes at 30-days of culture were grown for an additional 6 days in either control media, media containing Pinacidil or potassium gluconate (+ 25 mM). They were then given fresh control media and grown for another two days, then immediately prior to imaging, cells were stained with 50 nM VF2.1 and 1 µM Hoechst 33342 for 30-minutes in a humidified incubator at 37°C and 5% CO_2, washed twice with PBS and then given fresh keratinocyte media. Fluorescence Lifetime Imaging was performed with the Leica SP8 Confocal microscope. The collected FLIM images were fitted with biexponential decay curve in the Leica suit, thresholded to remove background, and exported as '.Tif' files for further analysis. Using a 15 x 15 pixels ROI was used to scan the image and generate an excel file containing 'X', 'Y', and 'Lifetime' for rois above 100% 'ON' pixels. To determine the appropriate 'k' value, i.e. number of clusters, for the Moran's I calculation, we initially ran an elbow test to trial k values from 1 – 10 and determined the elbow of the curve to be at k=3. To control for differences in cell number, we subsampled our data (1000 cells) with 10 iterations which was then averaged. (A) Pre-treatment with Pinacidil did not result in a significant change; however, potassium gluconate treatment significantly reduced Moran's I from 0.63 to 0.26 ($p<0.01$, control n=4 biological replicate, potassium gluconate n=4 biological replicate). (B-i) Scatter plot of Lifetime vs spatial lag Lifetime also revealed a more random distribution of points, consistent with reduced spatial autocorrelation. (C) Local Moran computation shows reduction in size and distribution of distinct clusters in potassium gluconate pre-treated cells. (D) representative images of VF2.1 stained cells showing corresponding clusters.

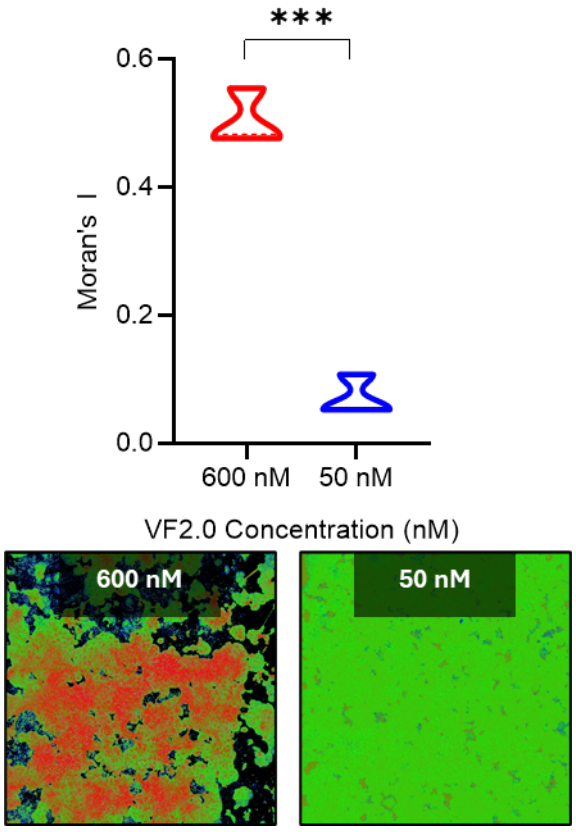

Supplementary Figure 1 – Control Dye VF2.0 Reveals Concentration Dependent Spatial Artifacts. Keratinocytes at 20-days of culture were stained with 600 nM or 50 nM VF2.0 for 30-minutes in a humidified incubator at 37°C and 5% CO_2, washed twice with PBS and then given fresh keratinocyte media. Fluorescence Lifetime Imaging was performed with the Leica SP8 Confocal microscope. The collected FLIM images were fitted with biexponential decay curve in the Leica suit, thresholded to remove background, and exported as '.Tif' files for further analysis. Using a 15 x 15 pixels ROI was used to scan the image and generate an excel file containing 'X', 'Y', and 'Lifetime' for rois above 100% 'ON' pixels. To control for differences in cell number, we subsampled our data (1000 cells) with 10 iterations which was then averaged. (A) Violin plot showing high spatial Moran's I of 0.50 in keratinocytes stained with 600 nM; however, reducing concentration to 50 nM resulted in a Moran's I of 0.04 ($p < 0.001$, n= 3 replicates). (B) Representative images showing artifactual clustering.